TOPOLOGICAL MATTER

Distinguishing a Majorana zero mode using spin-resolved measurements

Sangjun Jeon,[1]* Yonglong Xie,[1]* Jian Li,[1,2,3]* Zhijun Wang,[1]
B. Andrei Bernevig,[1] Ali Yazdani[1]†

One-dimensional topological superconductors host Majorana zero modes (MZMs), the nonlocal property of which could be exploited for quantum computing applications. We use spin-polarized scanning tunneling microscopy to show that MZMs realized in self-assembled Fe chains on the surface of Pb have a spin polarization that exceeds that stemming from the magnetism of these chains. This feature, captured by our model calculations, is a direct consequence of the nonlocality of the Hilbert space of MZMs emerging from a topological band structure. Our study establishes spin-polarization measurements as a diagnostic tool to distinguish topological MZMs from trivial in-gap states of a superconductor.

Localized Majorana zero modes (MZMs) are non-Abelian quasiparticles that emerge at the ends of one-dimensional topological superconductors and may be used as building blocks for future topological quantum computers (*1–3*). A variety of condensed matter systems can be used to engineer topological superconductivity and MZMs (*4–7*). To date, evidence for MZMs has come from experiments that have detected their zero-energy excitation signature in various spectroscopic measurements (*8–10*). However, despite the recent progress, the question as to whether a MZM could be distinguished from a finely tuned or accidental trivial zero-energy edge state in these experiments has been unresolved (*11–13*). The interpretation of the experimentally observed zero-energy modes as MZMs in various platforms has relied so far on showing that the zero-energy mode is detected when the parameters of the system make it most likely to be in a topological superconducting phase. Although there is intense interest in using such modes to create topological qubits [for example, (*14*)], arguably, a unique experimental signature of MZMs has yet to be reported. Here we describe how spin-polarized spectroscopic measurements (*15–21*) can be used to distinguish MZMs from trivial localized quasiparticles by identifying experimental features that are a direct consequence of the nonlocality of the Hilbert space of MZMs emerging from a topological band structure.

Previous studies have provided strong evidence that combining ferromagnetism in chains of Fe atoms with the large spin-orbit coupling interaction of the Pb(110) surface on which they are self-assembled gives rise to a proximity-induced topological superconducting phase. This phase exhibits strongly localized MZMs at both ends of these chains (*9*, *22–24*). High-resolution scanning tunneling microscopy (STM) studies have directly visualized MZMs, placed a stringent bound on their splitting (<45 μeV), shown evidence for the predicted equal electron-hole spectral weight using spectroscopy with superconducting tips, provided a detailed understanding of their spatial profile, and revealed the robustness of their signatures when the Fe chains are buried by the deposition of additional superconducting material on top (*25*). Because trivial zero-energy localized states may still show some of the features attributed to MZMs, we turned our attention to spin-polarized measurements of this system.

We performed spin-polarized STM (SP-STM) measurements (*26*) of self-assembled Fe chains by using Fe-coated Cr tips, which, although ferromagnetic at their apex, do not have strong enough magnetic fields to disrupt the superconductivity of the Pb(110) substrate [Fig. 1A, fig. S1, and section 1 of (*27*)]. Before making measurements in zero applied magnetic field, the tip's magnetization is first trained in situ with the application of a magnetic field that is either parallel (P) or antiparallel (AP) to the vector normal to the surface. We have found that the observation of the hard Bardeen-Cooper-Schrieffer (BCS) gap in the Pb substrate can be used to deduce whether or not trapped flux exists in our superconducting magnet. Often, by adding a small compensation field (~5 or −5 mT), the trapped flux can be canceled before proceeding with the spin-polarization measurement (fig. S2). The field training switches the orientation of the STM tip's magnetization relative to that of the Fe chains (*28*), which results in a change of the apparent height of the chains and a uniform shift of the topographic features, as shown in Fig. 1, B to D (see also fig. S5). The observation of two types of contrast in topographs of many different chains with the same spin-polarized tip confirms the ferromagnetic behavior of our chains (figs. S3 and S4). The height difference in the topographs reflects the difference between the "up" and "down" spin-polarized density of normal states ($\rho_N^{\uparrow}$, $\rho_N^{\downarrow}$) of the chains near the Fermi energy (E_F), the integral of which (between E_F and voltage bias eV_B) is related to the tunneling current, which is kept constant by the STM feedback loop. This compensation of $\delta\rho_N = \rho_N^{\uparrow} - \rho_N^{\downarrow}$ by the so-called STM set-point effect, for eV_B close to E_F, is best demonstrated by the spectroscopic measurements [$G(V) = dI/dV|_{eV=E} \propto \rho(E)$] of the Fe chains, such as in Fig. 1E, where a small 100-mT (out-of-plane) magnetic field is used to suppress superconductivity in Pb and Fe chains (G, differential conductance; V, voltage; I, current). The spectra measured at all locations on the chains near E_F with both tip orientations [$G_P(V)$, $G_{AP}(V)$] are equal, because the average spin polarization is compensated by adjusting the tip height for the two spectra [figs. S6 to S8 and sections 2 to 4 in (*27*)]. It is possible to avoid this compensation and to artificially enhance the influence of spin polarization on $G(V)$ by choosing a set-point bias that is further from E_F [figs. S1 and S3 and section 1 of (*27*)]. Previously, we have used this approach to demonstrate that our Fe chains are ferromagnetically ordered [30 meV in (*9*)]. However, for the purpose of the current study, we focused on a small bias window near E_F, where the normal state spin-dependent contribution is compensated by the STM set-point effect. As shown in Fig. 1F, the STM-measured spin polarization, $P(E) = [G_P(E) - G_{AP}(E)]/[G_P(E) + G_{AP}(E)]$, is zero over an energy window of ±5 meV. Repeating the same measurements in the superconducting state therefore allowed us to detect whether low-energy quasiparticle states show any spin polarization beyond that caused by the ferromagnetism of our atomic chains.

Our finding that the MZM shows a distinctive spin signature is demonstrated by measurements of the spin-polarized zero-bias conductance $G_P(0)$ and $G_{AP}(0)$ maps of the atomic chains in zero magnetic field (Fig. 2). The "double-eye" spatial structure of the MZM in such high-resolution maps at zero bias near the end of Fe chains has been previously measured with unpolarized tips (*25*). It is theoretically understood from model calculations that consider both the spectral weight of the MZM in the superconducting substrate and the trajectory of the STM tip during the constant current conductance map measurements. The data in Fig. 2, however, show that the magnitude of the MZM signature in $G_P(0)$ and $G_{AP}(0)$ maps depends on the magnetic polarization of the STM tip. Moreover, the contrast can be reversed by reorienting the tip's magnetization or by examining different chains with different ferromagnetic orientation [figs. S9 and S10 and section 5 of (*27*)]. $G_P(0)$ and $G_{AP}(0)$ maps do not show any contrast away from the end of the chain (dashed lines in Fig. 2C), where the signal in the bulk of the chain is likely dominated by the background from higher-energy quasiparticles in our system, owing to thermal broadening in our experiments (performed at 1.4 K). The spin contrast shown in Fig. 2, reproduced for many chains, demonstrates that the end zero mode in our system has a polarization beyond the normal-state background caused by the magnetism of the chains.

The details of the spin dependence of the tunneling conductance as a function of energy

[1]Joseph Henry Laboratories and Department of Physics, Princeton University, Princeton, NJ 08544, USA. [2]Institute for Natural Sciences, Westlake Institute for Advanced Study, Hangzhou, Zhejiang, China. [3]Westlake University, Hangzhou, Zhejiang, China.
*These authors contributed equally to this work. †Corresponding author. Email: yazdani@princeton.edu

and position throughout the chain can be found in Fig. 2, D to G, which, in addition to the spin polarization of the edge-bounded MZM, also shows the polarization of the other in-gap states at higher energies. These so-called Shiba states induced by magnetic structures on superconductors (*29*, *30*) are predicted to be spin-polarized (*30*, *31*); however, their spin properties have not been experimentally detected. To better characterize the spin polarization of both the MZM and the Shiba states in spectroscopic measurements, in Fig. 3, A and B, we show averaged spectra at the end and in the middle of the chain, along with the spin polarization $P(E)$ computed from these spectra. In addition to the MZM spin-polarization signature as a peak at $P(0)$, another key finding is the antisymmetric behavior of $P(E)$ for Shiba states at higher energies. These measurements demonstrate that the states with energy $|E| < \Delta_{Pb}$, where Δ_{Pb} is a superconducting gap, show features beyond those expected simply from the ferromagnetism of the chain, the average polarization of which is compensated by the STM set-point effect, as described above.

The first step in understanding that our spin-polarized measurements distinguish the presence of the MZM in our system is to show that no trivial localized state can give rise to a signal in the STM-measured $P(E)$ at zero energy. To illustrate this point, we consider a single magnetic impurity in a host superconductor (Fig. 4A), which gives rise to a localized Shiba state within the superconductor's gap (Δ_{Pb}) at $eV = \pm E_0 < \Delta_{Pb}$ (Fig. 4B). We have recently computed the spin properties of these states by using a model that considers a magnetic quantum impurity (for example, a partially filled d level) coupled to a host superconductor [(*32*) and section 6 of (*27*)]. The changes in the superconducting host's normal state $\rho_N^{\uparrow/\downarrow}$ induced by the magnetic impurity via the exchange interaction determine the spin polarization of the Shiba state inside the gap: $\rho_S^{\uparrow/\downarrow}(E) = \pi\rho_N^{\uparrow/\downarrow}\sqrt{\Delta_{Pb}^2 - E_0^2}\,\delta(E \mp E_0)$ (Fig. 4B).

From this result, we see that the polarization of a trivial localized Shiba state tuned to zero energy ($E_0 = 0$) is no larger than that of the normal-state polarization induced by the magnetic impurity. Moreover, it can be shown by symmetry that the spin contrast in our constant current conductance measurements [$\delta G(E) = G_P(E) - G_{AP}(E)$] for the localized Shiba state must be antisymmetric as function of energy [$\delta G(E) = -\delta G(-E)$], which means that there should be no spin contrast in spin-polarized STM measurements for $E_0 = 0$ Shiba states [(*32*) and section 6 of (*27*)]. Our observation of a spin contrast for the edge mode of our atomic chains therefore excludes the possibility that this zero-energy feature is caused purely by a localized Shiba state at zero energy. Because a Shiba state caused by magnetic impurities is the only known trivial mechanism able to produce a localized in-gap differential conductance peak that disappears in the absence of superconductivity, our observation of a localized peak in $P(E)$ at zero energy uniquely identifies the MZM in our chains.

To further show that our spin-polarization measurements distinguish between trivial quasiparticle states and the topological MZM, we compare our experimental results to model calculations of chains of magnetic impurities embedded in a superconductor [section 7 of (*27*)]. A chain of magnetic atoms induces a band of Shiba states within the host gap, which produces pairs of peaks at positive and negative bias in a $G(V)$ simulation (Fig. 3, C and D). The width of these peaks is related to the bandwidth of the Shiba states and their dispersion. For simplicity, we model a single Shiba band (Fig. 3, C and D), but previously we have shown that the shape of experimental spectra (Fig. 3, A and B) is captured by a model including multiple Shiba bands (*25*). The Shiba bands produce signatures in spin-polarized measurements that are very similar to that of a localized Shiba state. Specifically, the energy-antisymmetric feature in $P(E)$ that we have discussed above as being the hallmark of localized Shiba states also describes the behavior of extended Shiba states detected both at the ends and in the middle of the chains (Fig. 3, C and D). These features are reproduced in our experimental results (Fig. 3, A and B) and confirm our understanding of signatures in $P(E)$ arising from the extended Shiba states in our chains.

Our theoretical considerations of a hybrid chain-superconductor system also reveal that a larger polarization than that of the normal-state background, detected at zero energy in our experiments (Fig. 3A), is a diagnostic signature of the nonlocal nature of MZMs. Unlike trivial localized states, MZMs can only exist at the edge of a chain

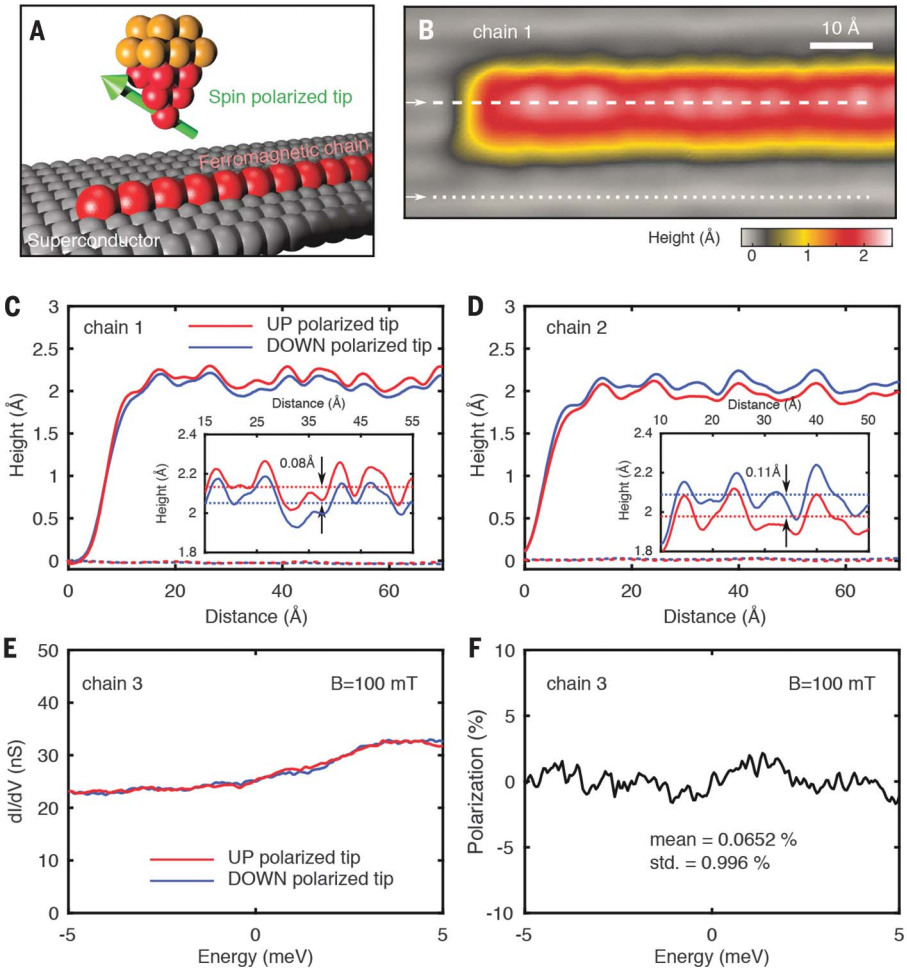

Fig. 1. Spin polarization of Fe chains on Pb(110) at normal state. (**A**) Schematic of the SP-STM measurement on a MZM platform probed by a Fe/Cr tip whose magnetization can be controlled by an external magnetic field (red, Fe; orange, Cr). (**B**) Topography of a typical Fe chain (chain 1) under zero magnetic field [set-point voltage (V_{set}) = 10 mV, set-point current (I_{set}) = 750 pA]. (**C** and **D**) Height profile of chain 1 (C) and chain 2 (D) measured with the up-polarized tip (solid red curves) and down-polarized tip (solid blue curves). Dashed lines show the height profiles of the Pb substrate measured with both tips. The positions of the topographic profiles are shown in (B). Insets show a magnification of the height profiles of the chains. Red and blue dashed lines in the insets show the average height of the chains measured with the up- and down-polarized tips, respectively. (**E**) Spectra measured in the middle of chain 3 at 100 mT with up-polarized (red curve) and down-polarized (blue curve) tips, which correspond to $G_P^N(V)$ and $G_{AP}^N(V)$ [V_{set} = −5 mV, I_{set} = 500 pA, modulation voltage (V_{mod}) = 40 μV]. (**F**) Calculated polarization of the spectra shown in (E).

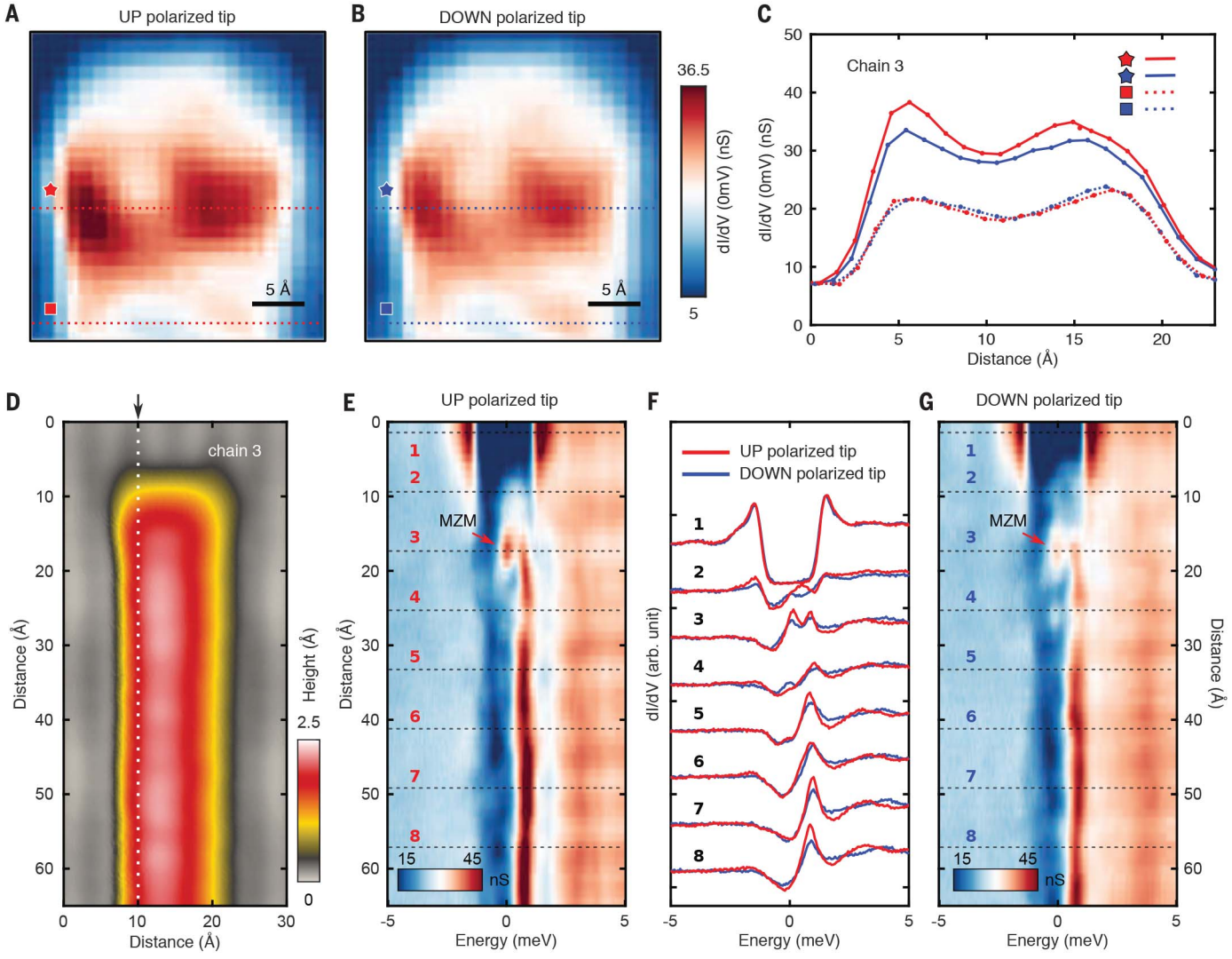

Fig. 2. Spatially resolved spin-polarized states on a Fe atomic chain. (**A** and **B**) Zero-energy conductance map near the chain end taken with up-polarized (A) and down-polarized (B) tips (V_{set} = −5 mV, I_{set} = 500 pA, V_{mod} = 40 μV). The conductance at the double-eye feature taken with the up-polarized tip (A) is stronger than that at the same feature taken with the down-polarized tip (B). (**C**) Line cuts taken from (A) and (B), as indicated by the corresponding symbols. Solid lines represent the conductance profile across the double-eye feature measured with up-polarized (red curves) and down-polarized (blue curves) tips. Dashed lines show typical conductance profiles away from the chain end. (**D**) Topographic image of chain 3 taken at zero external field (V_{set} = −10 mV, I_{set} = 750 pA). (**E** and **G**) Spatial variation of the spectra taken along the white dashed line shown in (D) with up-polarized (E) and down-polarized (G) tips (V_{set} = −5 mV, I_{set} = 500 pA, V_{mod} = 40 μV). (**F**) Individual spectra from (E) (red curves) and (G) (blue curves) at the labeled location. The end state appears at spectrum 3 (arb., arbitrary).

system with extended electronic states, the properties of which not only dictate the formation of MZMs, but also determine their spin polarization, as well as that of the normal-state background. Specifically, MZMs appear at the edges of ferromagnetic chains that have a normal-state band structure with an odd number of spin-split bands crossing E_F. The MZM in such chains emerges from only one of the spin-polarized bands at E_F and, in our case, is associated with the exchange-split d bands of the ferromagnetic Fe chains, as schematically shown in Fig. 4C. The large band splitting (~2 eV) between majority and minority bands in the Fe chains estimated in our previous study (*9*, *22*) guarantees that the minority spin bands cross E_F. The spin polarization of the MZM (Fig. 4D) is directly related to the spin polarization of these specific momentum states at E_F, where the induced topological gap is opened, although spin-orbit coupling results in a very slight tilting of the spin polarization away from the ferromagnetic magnetization. To understand why this localized MZM spin polarization can be detected in our STM measurements, we must contrast the MZM polarization with that of the normal-state background, which is compensated by the STM set-point effect. The normal-state background spin polarization of our system involves not only the Fe states crossing E_F, but also states further away in energy that are broadened owing to the hybridization with the Pb substrate (Fig. 4, C and D). The sum contribution of these delocalized states throughout the chain to the background at its end is always smaller than that of a localized MZM (*32*). Consequently, as our calculations for a hybrid chain-superconductor system show (Fig. 3C and 4D), the MZM spin polarization exceeds that of the normal-state background, providing an important test for the detection of MZMs in our system.

We contrast the nature of the background relevant to the MZM spin-polarization measurements with that of a trivial localized state, which may accidently appear near the end at near-zero energy. For such a localized state, as in the case of an isolated Shiba impurity (described above), the relevant normal-state background is local,

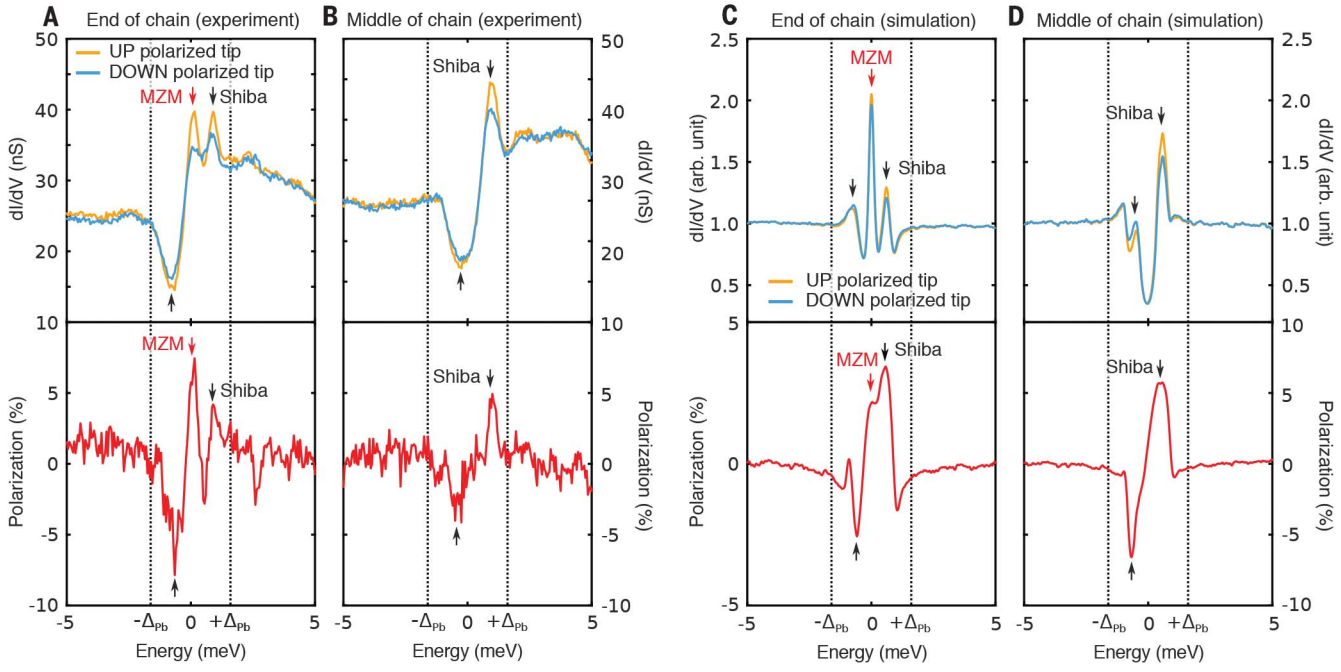

Fig. 3. Comparison of experimental data and SP-STS simulation. (**A** and **B**) Experimentally obtained spectra at the end of the chain (A) and in the middle of the chain (B) and their corresponding polarization (V_{set} = −5 mV, I_{set} = 500 pA, V_{mod} = 40 μV). Yellow and blue curves were measured with up- and down-polarized tips, respectively. Red arrows mark the zero-energy end state, and black arrows mark the Van Hove singularity of the Shiba band. (**C** and **D**) Simulated spectra at the end of the chain (C) and in the middle of the chain (D) and their polarization [section 7 of (*27*)]. Experimental and simulated results both show strong positive polarization for the end state and energetically antisymmetric polarization for the Shiba states at higher energies.

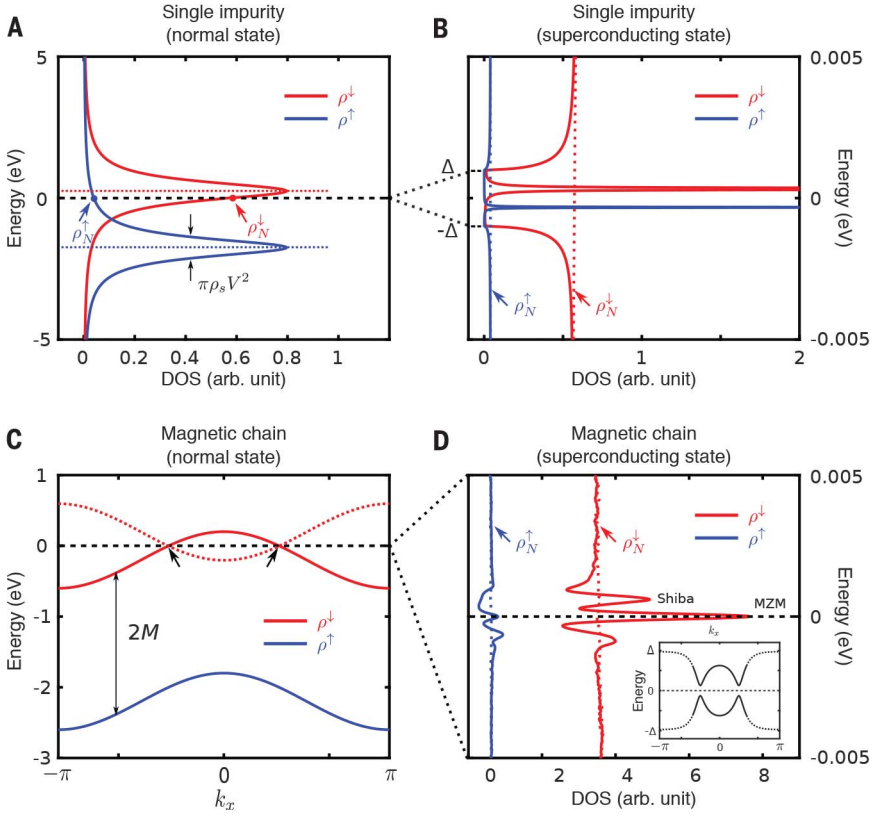

Fig. 4. Single magnetic impurity and magnetic chain model calculations. (**A** and **B**) Model calculation for a magnetic impurity hybridized with a superconductor [section 6 of (*27*) describes the model Hamiltonian used in this calculation: M = 1, μ = 0.75, ν = 0.4, Δ = 0.001, η = $5e^{-6}$]. The original d-orbital states of impurity are marked as dashed lines in (A) (red for the minority state and blue for the majority state). Solid curves represent the spin density of states (DOS) of the hybridized impurity-superconductor system. The width of DOS marked as $\pi\rho_s V^2$ is the broadening caused by the coupling between the magnetic impurity and the superconductor [section 6 of (*27*)]. A pair of Shiba states inside a superconducting gap is shown in (B). Dashed lines in (B) correspond to the normal-state spin DOS of the minority state (red) and majority state (blue), which are the same value as the spin DOS at the Fermi energy marked in (A). (**C** and **D**) Model calculation for a magnetic chain embedded in a superconductor [section 7 of (*27*)]. Solid curves in (C) are the dispersion of original d-orbital bands (red for the minority band and blue for the majority band, which are energetically split by the exchange energy 2*M*). The red dashed curve represents the hole copy of the minority band. Black arrows mark the momenta where the minority band crosses the Fermi level. Spin DOS calculated at the end of the chain displayed in (D) show MZM and Van Hove singularities of Shiba bands. Red and blue dashed lines are normal-state spin DOS of minority and majority bands, respectively. The inset shows the dispersion of Shiba bands. k_x is the wave vector along the magnetic chain.

resulting in compensation by the STM set-point effect and therefore showing no contrast in the spin-polarized measurements. A zero-energy peak in measurements of $P(E)$ in spin-polarized STM (Fig. 3A) is caused by the nonlocal nature of the MZM background and constitutes a unique signature of these excitations, allowing us to distinguish them from trivial edge modes.

Looking beyond our atomic-chain Majorana platform, spin-selective spectroscopy measurements using quantum dots have been recently proposed for the semiconducting nanowire Majorana platform (*33*). As we have done in this study for the atomic chains, such experiments are expected to distinguish between trivial and nontrivial edge modes and probe the nonlocal nature of MZMs in the nanowire platform. The spin polarization of MZMs may provide a useful approach to creating highly polarized spin currents and entangling these topological localized quantum states with conventional spin qubits. In fact, there are proposals outlining how a hybrid system of spin and MZM qubits can be used to perform universal quantum computation (*34*). The possibility that electron tunneling between spin qubits (based on quantum dots or individual defects) and MZMs can realize a quantum superposition between the two is intriguing. Such a process could, for example, facilitate long-distance entanglement between spatially well-separated spin qubits (*35*).

Note added in proof: After submission of our manuscript, a spin-polarized STM study of Co chains on Pb(110) was reported (*36*). The spin polarization of the Shiba bands on such chains also shows the antisymmetric features (with bias) and is consistent with our results and analysis.

REFERENCES AND NOTES

1. A. Y. Kitaev, *Phys. Uspekhi* **44**, 131–136 (2001).
2. C. Nayak, S. H. Simon, A. Stern, M. Freedman, S. Das Sarma, *Rev. Mod. Phys.* **80**, 1083–1159 (2008).
3. C. W. J. Beenakker, *Annu. Rev. Condens. Matter Phys.* **4**, 113–136 (2013).
4. L. Fu, C. L. Kane, *Phys. Rev. Lett.* **100**, 096407 (2008).
5. Y. Oreg, G. Refael, F. von Oppen, *Phys. Rev. Lett.* **105**, 177002 (2010).
6. R. M. Lutchyn, J. D. Sau, S. Das Sarma, *Phys. Rev. Lett.* **105**, 077001 (2010).
7. S. Nadj-Perge, I. K. Drozdov, B. A. Bernevig, A. Yazdani, *Phys. Rev. B* **88**, 020407 (2013).
8. V. Mourik *et al.*, *Science* **336**, 1003–1007 (2012).
9. S. Nadj-Perge *et al.*, *Science* **346**, 602–607 (2014).
10. S. M. Albrecht *et al.*, *Nature* **531**, 206–209 (2016).
11. E. J. H. Lee *et al.*, *Nat. Nanotechnol.* **9**, 79–84 (2014).
12. R. Žitko, J. S. Lim, R. López, R. Aguado, *Phys. Rev. B* **91**, 045441 (2015).
13. M. T. Deng *et al.*, *Science* **354**, 1557–1562 (2016).
14. D. Aasen *et al.*, *Phys. Rev. X* **6**, 031016 (2016).
15. D. Sticlet, C. Bena, P. Simon, *Phys. Rev. Lett.* **108**, 096802 (2012).
16. J. J. He, T. K. Ng, P. A. Lee, K. T. Law, *Phys. Rev. Lett.* **112**, 037001 (2014).
17. A. Haim, E. Berg, F. von Oppen, Y. Oreg, *Phys. Rev. Lett.* **114**, 166406 (2015).
18. K. Björnson, S. S. Pershoguba, A. V. Balatsky, A. M. Black-Schaffer, *Phys. Rev. B* **92**, 214501 (2015).
19. P. Kotetes, D. Mendler, A. Heimes, G. Schön, *Physica E Low Dimens. Syst. Nanostruct.* **74**, 614–624 (2015).
20. H. H. Sun *et al.*, *Phys. Rev. Lett.* **116**, 257003 (2016).
21. P. Szumniak, D. Chevallier, D. Loss, J. Klinovaja, *Phys. Rev. B* **96**, 041401 (2017).
22. J. Li *et al.*, *Phys. Rev. B* **90**, 235433 (2014).
23. M. Ruby *et al.*, *Phys. Rev. Lett.* **115**, 197204 (2015).
24. R. Pawlak *et al.*, *NPJ Quantum Inf.* **2**, 16035 (2016).
25. B. E. Feldman *et al.*, *Nat. Phys.* **13**, 286–291 (2016).
26. R. Wiesendanger, *Rev. Mod. Phys.* **81**, 1495–1550 (2009).
27. Supplementary materials.
28. Fe chains have a higher coercive field (>6 T), and their magnetization cannot be switched by applying a 1-T training field.
29. A. Yazdani, B. A. Jones, C. P. Lutz, M. F. Crommie, D. M. Eigler, *Science* **275**, 1767–1770 (1997).
30. A. V. Balatsky, I. Vekhter, J.-X. Zhu, *Rev. Mod. Phys.* **78**, 373–433 (2006).
31. C. P. Moca, E. Demler, B. Jankó, G. Zaránd, *Phys. Rev. B* **77**, 174516 (2008).
32. J. Li, S. Jeon, Y. Xie, A. Yazdani, B. A. Bernevig, The Majorana spin in magnetic atomic chain systems. arXiv:1709.05967 [cond-mat.mes-hall] (18 September 2017).
33. E. Prada, R. Aguado, P. San-Jose, *Phys. Rev. B* **96**, 085418 (2017).
34. S. Hoffman, C. Schrade, J. Klinovaja, D. Loss, *Phys. Rev. B* **94**, 045316 (2016).
35. M. Leijnse, K. Flensberg, *Phys. Rev. Lett.* **107**, 210502 (2011).
36. M. Ruby, B. W. Heinrich, Y. Peng, F. von Oppen, K. J. Franke, *Nano Lett.* **17**, 4473–4477 (2017).

ACKNOWLEDGMENTS

We acknowledge discussions with L. Glazman, F. von Oppen, K. Franke, P. Lee, and C. Kane. This work has been supported by the Gordon and Betty Moore Foundation as part of the EPiQS initiative (GBMF4530), the Office of Naval Research (grants ONR-N00014-14-1-0330, ONR-N00014-11-1-0635, and ONR-N00014-13-1-0661), NSF MRSEC (Materials Research Science and Engineering Centers) programs through the Princeton Center for Complex Materials (award DMR-1420541), NSF award DMR-1608848, a Simons Investigator Award, NSF EAGER (Early-concept Grants for Exploratory Research) award NOA-AWD-1004957, the Department of Energy's Office of Basic Energy Sciences, the Packard Foundation, Army Research Office MURI (Multidisciplinary University Research Initiatives) program W911NF-12-1-046, and the Eric and Wendy Schmidt Transformative Technology Fund at Princeton. This project was also made possible by the facilities at Princeton Nanoscale Microscopy Laboratory. B.A.B. thanks Ecole Normale Superieure, UPMC (Université Pierre et Marie Curie) Paris, and Donostia International Physics Center for their generous sabbatical hosting. A.Y. acknowledges the hospitality of the Aspen Center for Physics, supported by NSF award PHY-1607611. The data presented in this paper are available from the corresponding author upon reasonable request.

SUPPLEMENTARY MATERIALS

www.sciencemag.org/content/358/6364/772/suppl/DC1
Materials and Methods
Supplementary Text
Figs. S1 to S10

3 April 2017; accepted 29 September 2017
Published online 12 October 2017
10.1126/science.aan3670

Distinguishing a Majorana zero mode using spin-resolved measurements

Sangjun Jeon, Yonglong Xie, Jian Li, Zhijun Wang, B. Andrei Bernevig and Ali Yazdani

Science **358** (6364), 772-776.
DOI: 10.1126/science.aan3670originally published online October 12, 2017

Topological or trivial?

Evidence for Majorana bound states (MBS), which are expected to provide a platform for topological quantum computing, has been found in several material systems. Typically, the experimental signature is a peak in the spectrum at zero energy, but mechanisms other than MBS need to be carefully ruled out. Using spin-polarized scanning tunneling spectroscopy, Jeon *et al.* studied chains of iron atoms deposited on superconducting lead and found a more distinctive signature of the topological states. Unlike trivial zero-energy states, MBS exhibited a characteristic spin-polarization signal.

Science, this issue p. 772